Observation of H$_2$ $I^1\Pi_g^{+/-}$-$B^1\Sigma_u^+$ band spectra in a hollow-cathode glow discharge

Taiichi SHIKAMA and Shinichiro KADO[1)]

Department of Mechanical Engineering and Science,
Graduate School of Engineering, Kyoto University, Kyoto 606-8501, Japan
[1)]*Department of Nuclear Engineering and Management,*
School of Engineering, The University of Tokyo, Tokyo 113-8656, Japan

An excitation-emission model for the H$_2$ $I^1\Pi_g^{+/-} - B^1\Sigma_u^+$ transition has been developed based on the coronal equilibrium. Within the framework of the adiabatic theory, the vibronic transition probability is calculated instead of the Franck-Condon factor. The ro-vibrational temperatures are evaluated through the experiment carried out in a low-density hollow-cathode plasma. The evaluated temperatures are compared with those from the $d^3\Pi_u^{+/-} - a^3\Sigma_g^+$ (Fulcher-α) transition.

1. Introduction

The ro-vibrational excitation of hydrogen molecules largely affects the reaction rate of molecular relevant processes both in fusion and laboratory plasmas. In order to determine the rate coefficient, and to achieve active control of the excitation, the state resolved ro-vibrational population densities have been measured using several techniques based on laser [1–3] or passive emission [4–6] spectroscopies. Since diatomic molecules have no permanent electric dipolar moments, the spectroscopic measurement of the electronic ground state requires indirect methods via the excited states. In this case, it is necessary to rely on an appropriate excitation-emission modeling. The most electronic excited states of hydrogen molecules are, however, known to have perturbations, and these states cannot be analyzed by means of the adiabatic approximation. The remaining states described within the adiabatic theory are therefore of great interest for the ro-vibrational excitation diagnostics.

In the visible wavelength region, several transitions have been used to deduce the ro-vibrational temperatures [4,5,7–9]. In particular, the $d^3\Pi_u^{+/-} - a^3\Sigma_g^+$ transition, known as the Fulcher-α band, has been widely used. Based on the well-established dataset for the excitation-emission processes, coronal models were developed [5, 6]. Although a collisional-radiative model for the triplet states was also constructed [10, 11], it was reported that the similarity in the potential curve shapes among the d, a, and $X^1\Sigma_g^+$ states enables a modeling with the assumption of the coronal equilibrium even in the case of high electron density. Among the other transitions, the $I^1\Pi_g^{+/-} - B^1\Sigma_u^+$ transition lying in the 380-600 nm

author's e-mail: shikama@me.kyoto-u.ac.jp

region has relatively high emission intensity. One of the upper states $I^1\Pi_g^+$ is known to be perturbed by the adjacent $GK^1\Sigma_g^+$ and $J^1\Delta_g^+$ states [12], while the other $I^1\Pi_g^-$ state can be treated by the adiabatic theory without large errors [13, 14].

In this paper, we have performed an excitation-emission modeling of the $I - B$ transition on the basis of the recently developed coronal model [6,15]. Taking the dependence on the inter-nuclear distance into account, the vibronic transition probabilities were calculated. The ro-vibrational temperatures of the X state obtained from the $d - a$ and $I - B$ transitions were compared.

2. Coronal model

An excitation-emission model is developed by assuming the coronal equilibrium. As shown in Fig. 1, the electron-impact excitation from the X state to the I state balances the radiative de-excitation from the I state to the B, $C^1\Pi_u^{+/-}$, and $B'^1\Sigma_u^+$ states. In the figure, $+/-$ denotes the parity with respect to the space-fixed inversion, e/f denotes the e/f convention, and s/a denotes the symmetry and asymmetry with respect to the permutation of nuclei. The ro-vibronic transition intensity is expressed with Hund's case (b) notation as

$$I_{v''N''}^{v'N'} = h\nu_{v''N''}^{v'N'} n_{v'N'} A_{v''N''}^{v'N'}, \qquad (1)$$

where v and N are the vibrational and rotational quantum numbers, respectively, $h\nu_{v''N''}^{v'N'}$ is the photon energy, $n_{v'N'}$ is the upper state population density, and $A_{v''N''}^{v'N'}$ is the spontaneous emission coefficient. The double prime and prime denotes the I (or d) and B (or a) states, respectively. $A_{v''N''}^{v'N'}$ is defined as

$$A_{v''N''}^{v'N'} = \frac{16\pi^3}{3\epsilon_0 hc^3}\nu_{v''N''}^{v'N'}{}^3 \frac{|\langle\phi'|\mu_e|\phi''\rangle|^2}{2N'+1}, \qquad (2)$$

where μ_e is the transition electric dipolar moment, and $|\phi\rangle = |\phi_e\rangle|\phi_v\rangle|\phi_r\rangle$ is the total wavefunction divided into the electronic (e), vibrational (v), and rotational (r) wavefunctions. For hydrogen molecules, the electric dipolar moment is not a weak function of the inter-nuclear distance [6, 7, 16], then the factor $|\langle\phi'|\mu_e|\phi''\rangle|^2$ is written as

$$|\langle\phi'|\mu_e|\phi''\rangle|^2 = P_{v''N''}^{v'N'}S_{N''}^{N'}, \tag{3}$$

where $P_{v''N''}^{v'N'} = |\langle\phi_v'|\langle\phi_e'|\mu_e|\phi_e''\rangle|\phi_v''\rangle|^2$ is the vibronic transition probability (VTP), and $S_{N''}^{N'} = |\langle\phi_r'|\cos\theta|\phi_r''\rangle|^2$ is the Hönl-London factor.

Since the ro-vibrational temperatures in the excited states are not usually in the thermal equilibrium with those in the ground state, the excitation-emission modeling provides an association between the temperatures in both states. In the coronal equilibrium, the upper state population $n_{v'N'}$ is described as

$$n_{v'N'} = \frac{n_e\sum_{v,N}\left[n_{vN}\langle\sigma_e v_e\rangle_{v'N'}^{vN}\right]}{\sum_{v''N''}A_{v''N''}^{v'N'}}, \tag{4}$$

where n_e is the electron density. The variables not marked with the prime denote the X state. The spontaneous emission coefficients to the B, C, and B' states are summed for the $I-B$ transition, and those to the d state are summed for the $d-a$ transition. The population n_{vN} is expressed [17] as

$$n_{vN} = n_{v=0}\exp\left[-\frac{\Delta G(v)}{kT_{\text{vib}}}\right]$$

$$\times\ \frac{g_{\text{as}}(2N+1)\exp\left[-\frac{\Delta F(N,v)}{kT_{\text{rot}}}\right]}{\sum_N g_{\text{as}}(2N+1)\exp\left[-\frac{\Delta F(N,v)}{kT_{\text{rot}}}\right]}, \tag{5}$$

where $n_{v=0}$ is the population in the vibrational ground state, g_{as} is the nuclear-spin statistical weight, $\Delta G(v)$ and $\Delta F(N,v)$ are the vibrational and rotational energies from their ground states, respectively, and T_{vib} and T_{rot} are the vibrational and rotational temperatures of the X state, respectively. $\langle\sigma_e v_e\rangle_{v'N'}^{vN}$ is the electron-impact excitation rate coefficient, which can be approximated [6] as

$$\langle\sigma_e v_e\rangle_{v'N'}^{vN} = \langle\sigma_v v_e\rangle_{v'N'}^{vN}a_{N'}^N, \tag{6}$$

where $\langle\sigma_v v_e\rangle_{v'N'}^{vN}$ is the vibronic excitation rate coefficient, and $a_{N'}^N$ is the relative probability of the rotational transition. $\langle\sigma_v v_e\rangle_{v'N'}^{vN}$ is assumed to be equal to the Franck-Condon factor (FCF) multiplied by the rate coefficient

$$\langle\sigma_v v_e\rangle_{v'N'}^{vN} = q_{v'N'}^{vN}\int_{E_{\text{th}}}^\infty\sigma_e(E)v_e f_e(E)dE, \tag{7}$$

where $q_{v'N'}^{vN} = |\langle\phi_v|\phi_v'\rangle|^2$ is the FCF, E_{th} is the threshold energy of the excitation, $\sigma_e(E)$ is the vibrationally averaged electron-impact excitation cross section, and

$f_e(E)$ is the electron energy distribution function. It should be noted that the dependence on the inter-nuclear distance is neglected in eq. (7) since the transition is optically forbidden. The probability $a_{N'}^N$ can be expressed both for singlet-singlet [18] and singlet-triplet [19] transitions as

$$a_{N'}^N = \frac{1}{2}[1 + (-1)^{N+N'}]$$

$$\times\ \sum_r \bar{Q}_r(2N'+1)\left(\begin{array}{ccc} N' & r & N \\ 1 & -1 & 0 \end{array}\right)^2, \tag{8}$$

where $\bar{Q}_r$ is the normalized partial cross section which satisfies $\sum_r\bar{Q}_r = 1$.

3. Experiment

An experiment was carried out using a hollow-cathode discharge chamber at the University of Tokyo. The details of the setup are described in elsewhere [20]. Briefly, the device consisted of a copper anode and an aluminum cathode. The cathode had face-to-face twin holes for diagnoses. In the present experiment, a dc-glow discharge with a discharge voltage of 295 V and discharge current of 70 mA was sustained. The background gas pressure measured by a Baratron gauge was 13 Pa, and the atomic fraction was less than a few percent. The electron temperature and density measured by a double probe was 3.1 eV and 5.4 $\times$ 10^{16} m^{-3}, respectively. The emission from the plasma was collected using an objective lens with a spot size of approximately 10 mm in diameter at the center of the cathode. The collected emission was dispersed using a Czerny-Turner mounted spectrometer with a focal length of 1 m and 2400 grooves/mm holographic grating. The dispersed spectrum was detected using a cooled photomultiplier tube (PMT) detector (Hamamatsu R928). The PMT consisted of a multi-alkali
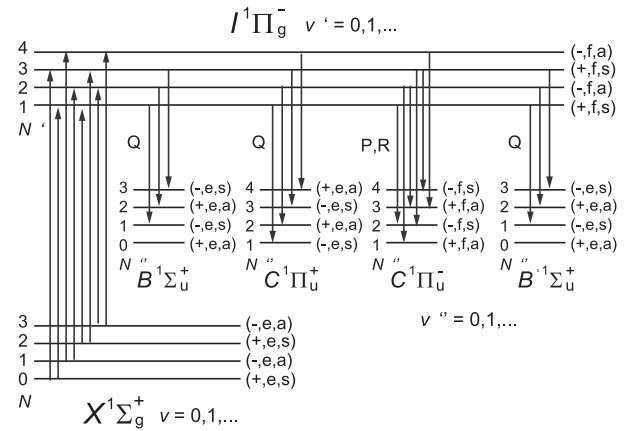

Fig. 1 Schematic diagram of the coronal equilibrium among the $X^1\Sigma_g^+$, $B^1\Sigma_u^+$, $C^1\Pi_u^{+/-}$, $B'^1\Sigma_u^+$, and $I^1\Pi_g^-$ states.

photocathode and UV glass envelope with the applicable wavelength range of 185-900 nm. The slit width of the spectrometer was set to 80 μm corresponding to a wavelength resolution of $\Delta\lambda_{\mathrm{fwhm}} = 0.023$ nm. The sensitivity of the spectroscopic system was absolutely calibrated using a tungsten lamp.

4. Results and Discussion
4.1 Dataset for excitation-emission modeling

The vibrational wavefunction was numerically calculated from the Schrödinger equation taking the vibration-rotation interaction [21] into consideration. The non-dimensionalized radial Schrödinger equation can be expressed as

$$\frac{d^2\phi_v(x)}{dx^2} +$$
$$\left[E - V(x) - \frac{B_0 N(N+1)}{x^2}\right]\frac{\phi_v(x)}{B_0} = 0, (9)$$

where E is the energy of the ro-vibrational state, and V is the adiabatic potential. B_0 and x are defined as $B_0 = h/8\pi^2 c\mu R_0^2$ and $x = R/R_0$, where μ is the reduced mass, R is the inter-nuclear distance, and R_0 is a normalization constant. The adiabatic potential curves were obtained from references: X [22], B [23], C [24], B' [23], I [25], a [26], d [26]. Eq. (9) was then numerically solved using the fourth-order Runge-Kutta method combined with the bisection algorithm. A calculation step of $\Delta x = 0.0001$ a.u. was used to obtain the optimal computational accuracy.

The VTP and FCF were calculated by Simpson's method with the electric dipolar moments for the $I - B$ [13], $I - C$ [13], $I - B'$ [13], and $d - a$ [26] transitions. The discrete data of the dipolar moments was interpolated using the cubic-spline curve over the inter-nuclear distance affecting the integral, as shown in Fig. 2. In the figure, the dependence of the transition moment on the inter-nuclear distance is clear. We confirmed that the calculated VTP and FCF for the $d - a$ transition ($N' = N'' = 0$) agree well with the precedent results [6]. The VTP for the $I - B$ transition normalized to the FCF ($v' = v'' = 0$) is shown in Tab. 1. The value in the bracket indicates the ratio $P_{v''0}^{v'0}/q_{v''0}^{v'0}$. The difference between the VTP and FCF is as large as 50% for the dominant transitions. Furthermore, because of the difference in the potential curve shapes of the I and B states, the effect of the vibration-rotation interaction is significant in the case of the $I - B$ transition. In Tab. 2, the effect with respect to N is shown.

The electron-impact excitation cross sections $\sigma_e(E)$ evaluated in [27] were used to determine the excitation rate coefffcient. The experimentally evaluated $a_{N'}^N$ are given in [19]. The corresponding value of $\bar{Q}_r$ for the $X - d$ excitation is $\bar{Q}_{r(X-d)} =$
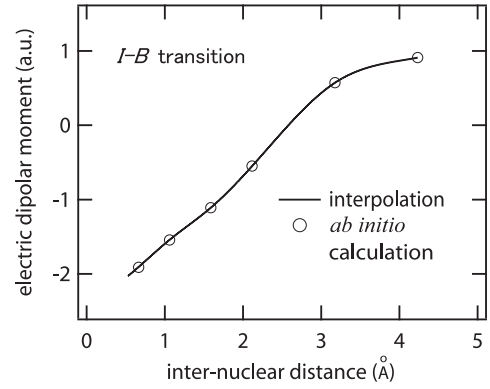

Fig. 2 Electric dipolar moment for the $I^1\Pi_g^{+/-} - B^1\Sigma_u^+$ transition. The *ab initio* calculation data was obtained from [13].

$\{0.76, 0.122, 0.1, 0.014\}$. In the reference, they applied least squares fitting to the measured d-state population densities in order to determine $\bar{Q}_r$. Since only the experimental data of $a_{N'}^1$ is available for the $X - I$ excitation, we performed the least squares fitting of eq. (8) to $a_{N'}^1$ by excluding the nuclear-spin selection rules. Although this procedure is different from that adopted in the reference, the descrepancy in the obtained $\bar{Q}_r$ values for the $X - d$ excitation is not significant: $\bar{Q}_{r(X-d:\text{this work})} = \{0.800, 0.162, 0.030, 0.008\}$. Moreover, it should be noted that the evaluation of $a_{N'}^1$ was carried out using both $\Pi^\pm$ states [19]. The lifetimes of all the transitions were, however, measured experimentally, and thereby errors caused by the perturbation may not be large. $\bar{Q}_r$ for the $X - I$ excitation estimated by this procedure resulted in $\bar{Q}_{r(X-I:\text{this work})} = \{0.434, 0.320, 0.121, 0.094, 0.031\}$. The cutoff value of r was determined so as to give the least χ^2 of the fitting. Fig. 3 shows that $a_{N'}^1$ decreases slowly with respect to N' for the $X - I$ excitation, namely, the rotation is excited to the I state more efficiently than to the d state.

4.2 Evaluation of ro-vibrational temperatures

An emission spectrum was continuously recorded in the range of 380-660 nm, and the absolute wavelength was calibrated using the Balmer series. In this wavelength range, several H_2 bands were able to be observed, and assignment was performed using Dieke's wavelength table [28]. After carefully excluding possibly contaminated lines, the observed number of PQR-branches (P, Q, R) was (15, 26, 12) for the $d - a$ transition and (19, 34, 15) for the $I - B$ transition. Because of the perturbations both on $d^3\Pi_u^+$ and $I^1\Pi_g^+$ states, only the Q-branch was used for the analysis. The higher rotational levels ($N \geq 6$) were omitted because of the presence of the super-thermal population [3,4].

Table 1 Calculated VTP in the case of $N' = N'' = 0$. The value in the bracket is the ratio $P_{v''0}^{v'0}/q_{v''0}^{v'0}$.

v''	$v' = 0$	1
0	0.512 (1.00)	0.287 (0.77)
1	0.356 (1.16)	0.050 (0.89)
2	0.161 (1.32)	0.246 (1.08)
3	0.061 (1.50)	0.227 (1.22)
4	0.021 (1.70)	0.132 (1.38)
5	0.007 (1.94)	0.062 (1.55)
	$v' = 2$	3
0	0.060 (0.57)	0.004 (0.32)
1	0.265 (0.68)	0.105 (0.47)
2	0.005 (1.12)	0.177 (0.56)
3	0.092 (1.00)	0.043 (0.96)
4	0.184 (1.15)	0.018 (0.96)
5	0.160 (1.29)	0.111 (1.07)

Table 2 Effect of the vibration-rotation interaction on the VTP. The value in the bracket is the ratio $P_{0N''}^{0N''}/P_{01}^{01}$.

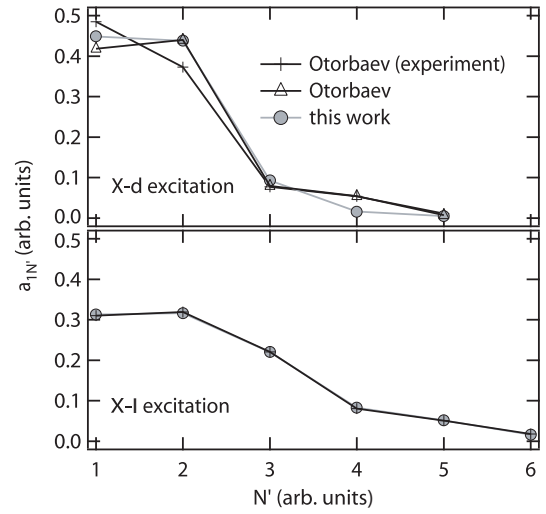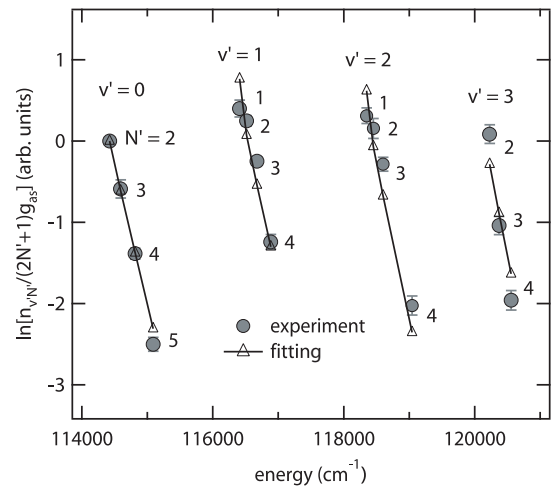| N''	$P_{B0N''}^{I0N''}$	$P_{a0N''}^{d0N''}$
1	0.510 (1.00)	0.931 (1.00)
2	0.505 (0.99)	0.934 (1.00)
3	0.497 (0.98)	0.937 (1.01)
4	0.488 (0.96)	0.942 (1.01)
5	0.476 (0.93)	0.948 (1.02)

Fig. 3 Relative rotational transition probability given in [19] (Otorbaev (experiment)). Calculated values using the $\bar{Q}_r$ given in the reference (Otorbaev). Calculated values using the $\bar{Q}_r$ obtained in this work (this work).

The X state ro-vibrational temperatures were measured by fitting eq. (4) to the experimentally obtained upper state populations. We assume that the generated plasma has a sufficiently low electron density to allow the application of the coronal model. The most probable ro-vibrational temperatures were determined with discrete temperature steps of 10 K for $T_{\rm vib}$ and 1 K for $T_{\rm rot}$ so as to minimize χ^2. Here, $\chi^2 = [(n_{v'N'(\rm exp.)} - n_{v'N'(\rm cal.)})/\sigma_{n_{v'N'(\rm exp.)}}]^2$, where $n_{v'N'(\rm exp.)}$ and $n_{v'N'(\rm cal.)}$ are the upper state populations obtained from the experiment and calculation, respectively, and $\sigma_{n_{v'N'(\rm exp.)}}$ is the standard deviation of $n_{v'N'(\rm exp.)}$. Errors were estimated over a temperature range chosen such that $\Delta\bar{\chi}^2 = 1$, where $\bar{\chi}^2$ is the reduced χ^2. In Fig. 4, the measured $I^1\Pi_g^-$ state population densities divided by the degeneracy are plotted along with the fitting results. The filled circles denote the experimentally measured populations, and the open triangles denote the fitting results. $n_{v'N'}$ obtained from the different vibronic transitions were averaged, and the population with $v' = 0$ and $N' = 2$ was normalized to unity. The ro-vibrational temperatures obtained from the $d - a$ and $I - B$ transitions are shown in Tab. 3. The semi-empirical calculation of the lifetime of the $I^1\Pi_g^-$ state [14] revealed that the lifetimes of the states with $0 \leq v' \leq 2$ are almost constant. Those of the states with $v' = 3$ are, however, slightly longer. Fitting without $v' = 3$ states was also performed, and the results are shown in Tab. 3. The obtained results indicate a slightly low $T_{\rm vib}$, which is the opposite tendency with respect to the lifetime, so that for the $v' = 3$ states the effect of the lifetime is not of much account compared to experimental errors.

Consequently, $T_{\rm rot}$ evaluated from the $I - B$ transition is close to that from the $d - a$ transition, while $T_{\rm vib}$ is substantially higher. The slight difference in

Fig. 4 Measured $I^1\Pi_g^-$ state population densities and the coronal model fitting results.

Table 3 Evaluated $X^1\Sigma_g^+$ state ro-vibrational temperatures.

	$d^3\Pi_u^- - a^3\Sigma_g^+$	$I^1\Pi_g^- - B^1\Sigma_u^+$ [w/o $n_{3N'}$]
T_{vib}	1730^{+170}_{-200} (K)	3330^{+370}_{-410} [3150^{+350}_{-410}] (K)
T_{rot}	417^{+14}_{-15} (K)	523^{+42}_{-38} [554^{+36}_{-44}] (K)

T_{rot} may originate from an error in the evaluated coefficient $a_{N'}^1$ for the $X - I$ excitation, as suggested in [4]. The reason for the discrepancy of T_{vib} is not clear at present. Possible causes may be the use of the excitation rate coefficient not including the dependence on the inter-nuclear distance, or deviation from the coronal equilibrium. Further verification of these points is required.

5. Conclusion

An excitation-emission model based on the coronal equilibrium was developed for the H$_2$ $I^1\Pi_g^{+/-} - B^1\Sigma_u^+$ transition. Because of the strong dependence of the transition electric dipolar moment on the inter-nuclear distance, the vibronic transition probability was calculated instead of the Franck-Condon factor. By considering the effect of the vibration-rotation interaction, the resultant transition probability was found to be substantially different from the Franck-Condon factor. The evaluated $X^1\Sigma_g^+$ state ro-vibrational temperatures were compared with those from the $d^3\Pi_u^- - a^3\Sigma_g^+$ transition. These rotational temperatures were similar, while the vibrational temperature obtained from the $I - B$ transition was higher. The cause of this discrepancy as well as dependence on the experimental conditions should be investigated further.

[1] R. F. G. Meulenbroeks, R. A. H. Engeln, J. A. M. van der Mullen, and D. C. Schram, *Phys. Rev. E* **53**, 5207 (1996).
[2] G. C. Stutzin, A. T. Young, H. F. Döbele, A. S. Schlachter, and K. N. Leung, *Rev. Sci. Instrum.* **61**, 619 (1989).
[3] T. Mosbach, H-M. Katsch, and H. F. Döbele, *Phys. Rev. Lett.* **85**, 3420 (2000).
[4] S. A. Astashkevich, M. Käning, E. Käning, N. V. Kokina, B. P. Lavrov, A. OHL, and J. Röpcke, *J. Quant. Spectrosc. Radiat. Transfer* **56**, 725 (1996).
[5] U. Fantz and B. Hegger, *Plasma Phys. Control. Fusion* **40**, 2023 (1998).
[6] B. Xiao, S. Kado, S. Kajita, and D. Yamasaki, *Plasma Phys. Control. Fusion* **46**, 653 (2004).
[7] U. Fantz, B. Schalk, and K. Behringer, *New J. Phys.* **2**, 7.1 (2000).
[8] S. A. Astashkevich, M. V. Kalachev, B. P. Lavrov, and V. L. Ovchinnikov, *Opt. Spec.* **87**, 203 (1999).
[9] H. N. Chu, E. A. Den Hartog, A. R. Lefkow, J. Jacobs, L. W. Anderson, M. G. Lagally, and J. E. Lawler, *Phys Rev. A* **44**, 3796 (1991).
[10] P. T. Greenland, *Proc. R. Soc. Lond. A* **457**, 1821 (2001).
[11] P. T. Greenland, *Contrib. Plasma Phys.* **42**, 608 (2002).
[12] S. Yu and K. Dressler, *J. Chem. Phys.* **101**, 7692 (1994).
[13] K. Dressler and L. Wolniewicz, *Can. J. Phys.* **62**, 1706 (1984).
[14] S. A. Astashkevich and B. P. Lavrov, *Opt. Spectrosc.* **85**, 379 (1998).
[15] T. Shikama, S. Kado, H. Zushi, and S. Tanaka, *Phys. Plasmas* **14**, 072509 (2007).
[16] U. Fantz and D. Wünderlich, *At. Data Nucl. Data Tables* **92**, 853 (2006).
[17] J. Tatum, *Astrophys. J. Suppl.* **14**, 21 (1967).
[18] B. P. Lavorv, V. N. Ostrovsky, and V. I. Ustimov, *J. Phys. B* **14**, 4389 (1981).
[19] N. N. Sobolev, "Elecron-excited molecules in nonequilibrium plasma" *Nova Science* pp. 121-173 (1989).
[20] D. Yamasaki, S. Kado, B. Xiao, Y. Iida, S. Kajita, and S. Tanaka, *J. Phys. Soc. Jpn.* **75**, 044501 (2006).
[21] D. Villarejo, R. Stockbauer, and M. G. Inghram, *J. Chem. Phys.* **50**, 1754 (1969).
[22] L. Wolniewicz, *J. Chem. Phys.* **99**, 1851 (1993).
[23] G. Staszewska and L. Wolniewicz, *J. Mol. Spec.* **212**, 208 (2002).
[24] L. Wolniewicz and G. Staszewska, *J. Mol. Spec.* **220**, 45 (2003).
[25] W. Kolos and J. Rychlewski, *J. Mol. Spec.* **66**, 428 (1977).
[26] G. Staszewska and L. Wolniewicz, *J. Mol. Spec.* **198**, 416 (1999).
[27] R. K. Janev, D. Reiter, and U. Samm, "Collision processes in low-temperature hydrogen plasmas" *Forschungszentrum Jülich Report*, Jül-4105 (2003).
[28] H. M. Crosswhite, "The hydrogen molecule wavelength tables of Gerhard Heinrich Dieke" *Wiley-Interscience* (1972).